Effect of heat treatment on the properties of wood-derived biocarbon structures

Min Yu[1,2], Theo Saunders[1,2], Taicao Su[1,2], Francesco Gucci[1,2], Michael John Reece[1,2,*]

[1]School of Engineering and Material Science, Queen Mary University of London, London E1 4NS, UK

[2]Nanoforce Technology Limited, London E1 4NS, UK

Abstract

Wood-derived porous graphitic biocarbons with hierarchical structures were obtained by high-temperature (2200-2400ºC) non-catalytic graphitization, and their mechanical, electrical and thermal properties are reported for the first time. Compared to amorphous biocarbon produced at 1000°C, the graphitized biocarbons-2200°C and -2400°C exhibited increased compressive strength (~36MPa) by ~38%, increased electrical conductivity (~29S/cm) by ~8 fold, and increased thermal conductivity (~9.5 W/(m·K)@800°C) by ~5 fold. The increase of duration time at 2200°C contributed to increased thermal conductivity by ~12%, while the increase of temperature from 2200 to 2400°C did not change their thermal conductivity, indicating that 2200°C is sufficient for non-catalytic graphitization of wood-derived biocarbon.

Keywords: graphitization, wood-derived biocarbon, thermal conductivity

1. Introduction

Wood-derived biocarbon (biochar, charcoal) structures have gained much attention owing to the hierarchical architecture of their cellular pore structures and the ability to produce complex shapes [1-4]. The graphitization of carbon has a significant impact on its properties, i.e. the electronic, magnetic and thermal properties [5-7]. Graphitic porous biocarbon monoliths are promising because they combine good mechanical properties at low density (0.11-0.97 g/cm^3) with the properties of graphite (high degree of ordering, low thermal expansion coefficient, good thermal and electrical conductivities) [8]. Two main techniques have been used to graphitize wood-derived biocarbons, including non-catalytic high-temperature (up to 3000°C) graphitization [5], and low-temperature (1300-1600°C) catalytic graphitization with Fe, Co, Mn and Ni etc [8-12]. During the catalytic graphitization process, the catalysts introduce impurities (i.e. carbides, metal particles) into the biocarbon structure, and the graphitic carbon surrounding the catalyst particles (i.e. Fe, Co, and Ni), can be formed at 1000-1600°C [8, 13]. Acid washing (i.e. HNO_3) is required to remove metal particles, in order to achieve pure graphitic carbon. Byrne et al. [14] graphitized wood-derived biocarbon at 2500°C without the use of a catalyst, however, they did not report their mechanical properties, electrical and

* Corresponding author: Michael J. Reece, Tel/Fax: +44(0)20 7882 2773
School of Engineering and Materials Science,
and Nanoforce Technology Limited, Queen Mary, University of London
Mile End Road, London E1 4NS
E-mail: m.j.reece@qmul.ac.uk

thermal conductivities. Until now, there are few reported works on the effect of temperature and duration time on the properties (especially thermal conductivity) of graphitized wood-derived biocarbon structures prepared by non-catalytic high-temperature (above 2000°C) graphitization [5].

Porous carbon materials with high thermal conductivity are needed for thermal energy storage, such as thermal enhancer and containers for phase change materials [15, 16]. Rico et al. [8] evaluated the thermal conductivity of Fe-catalyst graphitized wood-derived carbon, and found that the thermal diffusivity of graphitized carbon increased with increasing pyrolysis temperatures up to 800°C, mainly resulting from an increased degree of graphitization. Johnson et al. [17] found that Ni-catalyst graphitized wood-derived carbon has similar properties, and they further infiltrated copper into the pore structures to increase the thermal conductivity.

In this work, graphitized porous biocarbon monoliths derived from beech wood were obtained by heating at high temperatures (2200-2400ºC) without the use of a catalyst. This heat treatment was performed in a Spark Plasma Sintering (SPS) furnace with high heating and cooling rates (up to 200 ºC/min). Accordingly, we report for the first time the effects of temperature and duration time on the properties (compressive strength, electrical and thermal conductivity) of these samples prepared by non-catalytic high temperature graphitization.

2. Experimental process

Cylindrical pieces of beech wood (DOW003100, Tilgear Ltd, UK) were chosen as the carbon source. The cylindrical biocarbon structures (Ø=~6mm, H=~9mm) were prepared by pyrolyzing the beech wood (DOW003100, Tilgear Ltd, UK) at 1000 °C for 4h, as performed in our previous work [18]. The prepared biocarbon structures were then heated to higher temperatures (2200°C and 2400°C) in Ar for different duration times (2-15min) in a SPS furnace. A heating rate of 200°C/min and cooling rate of 100°C/min were used during this thermal processing. A pressureless mode in SPS was used in order to retain the porous biomorphic structure derived from the wood. The bulk density (geometrical density which includes pores) of the samples was estimated by dividing the weight by the geometrical volume. The solid density (which excludes the pores) of the samples was measured using the Archimedes' method.

An FEI Inspect-F scanning electron microscope (SEM, Hillsboro, OR) was used to characterize the morphology of the samples. Transmission electron microscopy (TEM) and X-ray diffraction (XRD, Siemens Diffraktometer-D5000, Germany) analysis with Cu Kα radiation were used to detect the crystalline structures in the samples. Raman spectroscopy (Horiba Jobin-Yvon) at room temperature was used to determine the degree of structural disorder in the carbons using an excitation of 514 nm. The degree of crystallinity (β) was calculated using the following equation [8]:

$$\beta = \frac{I_G}{I_G + I_D} \qquad \text{Eq.1}$$

Where I_G and I_D are the intensities (area under the peak) of the bands G (~1580cm^{-1}) and D (~1350cm^{-1}) in the Raman spectra, respectively.

The nitrogen absorption-desorption isotherm was measured using an Autosorb-IQ2-MP-C system (Quantachrome Instruments, USA). The specific surface area and pore size distribution were calculated using the multipoint Brunauer-Emmett-Teller (BET) method and Quenched Solid Density Function Theory (QSDFT), respectively.

The compressive strength of a set of six samples with nominal dimensions of Ø = 6±0.1 mm and H = 9±0.3 mm was measured in the axial direction at room temperature using a universal testing device (Instron, Model 4202, Instron Corp., Canton, MA). The displacement speed was set at 0.5 mm/min.

The room-temperature electrical conductivity of the samples was measured using a two-point conductivity measurement technique, using a picoameter (Keithley 6485) and DC voltage source (Agilent 6614C).

The thermal diffusivity (α) was measured on cylinder samples (diameter: ~6mm, thickness: ~1.5mm) using a Netzsch LFA-457 thermal analyzer. Three measurements were carried out at each temperature in the range of 25-800ºC in a flowing Ar atmosphere. The thermal conductivity (κ) was calculated using the following equation: $\kappa = C_p \times D \times \alpha$. In our work, the specific heat capacity (C_p) of samples was taken from the literature (0.25-2.0 J/(g·K) in the temperature range of 25 to 800°C) [19], and D was taken as the bulk density (geometric density).

3. Results and discussions

Fig.1 shows the microstructures and pore size distributions of the wood-derived biocarbons after different heat treatments. The biocarbon-2400°C exhibited uniform and nearly round macropores with diameters of ~30μm and ~8μm, as shown in Fig.1a and b. Dense struts (Fig.1c) were also observed, providing strong mechanical support for the structures. The biocarbon-1000ºC (Fig.1d) exhibited a relatively wide range of micropores (0-25nm), while the graphitized biocarbon-2400ºC exhibited a micropore distribution mainly concentrated in the range of 0-10nm (Fig.1e). This might result from the shrinkage of large nano-sized pores (10-50nm) during the graphitization process. In addition, the specific pore volume and specific surface area of the biocarbon-2400ºC were two orders of magnitude smaller than that of the biocarbon-1000 ºC, indicating the disappearance of micropores during the high temperature (2400ºC) treatment. This mainly resulted from the disappearance of small pores (≤50nm) caused by the rearrangement of carbon structures at high temperatures up to 2400 ºC. The shrinkage of nano-sized pores might limit the application of the graphitized biocarbon in the electrochemical energy storage application.

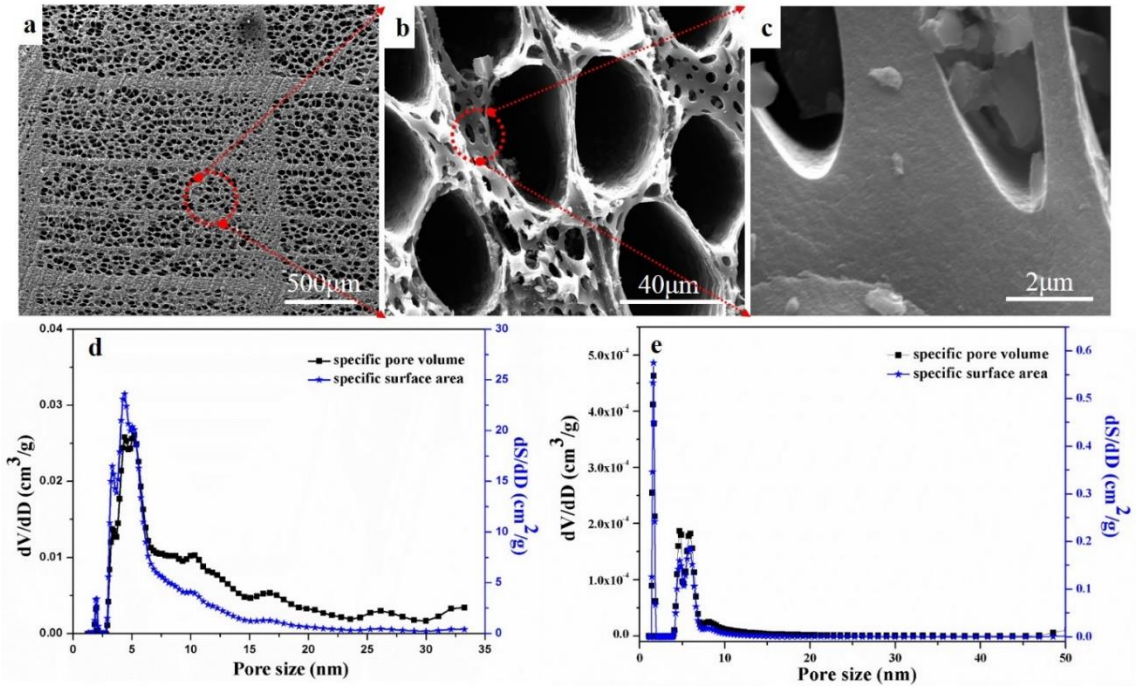

Fig.1. (a-c) SEM micrographs and (d and e) pore size distributions (based on BET analysis) of the biocarbon structures obtained at different heat treatment conditions. (a-c) and (d) are the sample prepared at 2400°C for 10min; (e) is the sample prepared at 1000°C for 4h.

The Raman spectra for the biocarbon-1000ºC exhibited a broad weak D peak at 1360cm^{-1} and G peak at 1584cm^{-1}, indicating that it contained little graphitic carbon (Fig. 2). All of the biocarbons prepared at 2200ºC and 2400ºC exhibited both a sharp D and G peak, which are related to the defect structure of graphite and perfect graphite structure (in-plane stretching of graphite lattice, in-plane vibration of sp^2 carbon atoms), respectively. The G/D ratio increased in the graphitized biocarbon-2200 ºC with the dwell time increasing from 2 to 15min. This indicates a higher degree of graphitization in the biocarbon, which is further confirmed by the XRD patterns (Fig.3a) and TEM images (Fig.3b and c). The biocarbon-2400ºC exhibited a slightly higher G/D ratio compared to the biocarbon-2200 ºC. Both biocarbon-2200 ºC and biocarbon-2400 ºC exhibited a smaller (~50%) full width at half maximum (FWHM) of their G band compared with biocarbon-1000°C, indicating a high relative amount of graphitic carbon to amorphous carbon. The corresponding crystalline ratio of the samples was calculated based on the Eq.1, and is shown in Table 1.

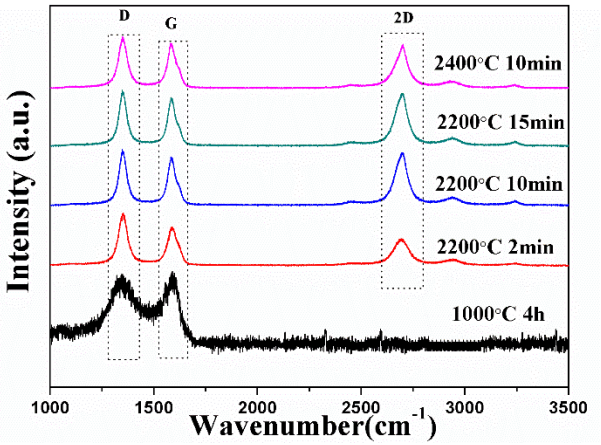

Fig.2. Raman spectra of wood-derived biocarbon prepared at different temperatures and dwell times.

The XRD and TEM analysis were also used to further investigate the graphitization of the biocarbons, as shown in Fig.3. The biocarbon-1000 ºC exhibited two broad peaks at 2θ=20-26° and 2θ=41-46°, which are characteristic of amorphous carbon. Both the biocarbon-2200 ºC and biocarbon-2400 ºC showed a superposition of two peaks (a broad peak and a sharp peak) at 2θ=20-28°. Both the biocarbon-2200 ºC and biocarbon-2400 ºC showed characteristic peaks at 2θ=26° and 2θ=43°, which correspond to the reflections of the (002) and (001) planes of graphitic carbon, respectively [20, 21], indicating the formation of graphitic carbon, which is in good agreement with the Raman data (Fig.2). The biocarbon-1000ºC exhibited a typical HRTEM image for an amorphous structure (Fig.3b), while the biocarbon-2400 ºC showed graphitic carbon layers (see red dashed circle) and some amorphous carbon regions (see red solid circle in Fig.3c). The SAED pattern (inset of Fig.3b) further confirmed the amorphous nature of biocarbon-1000ºC, which is consistent with the XRD data (Fig.3a). The SAED pattern (inset of Fig.3c) further confirmed the crystallinity of the biocarbon-2400ºC, consistent with the peaks in the XRD pattern.

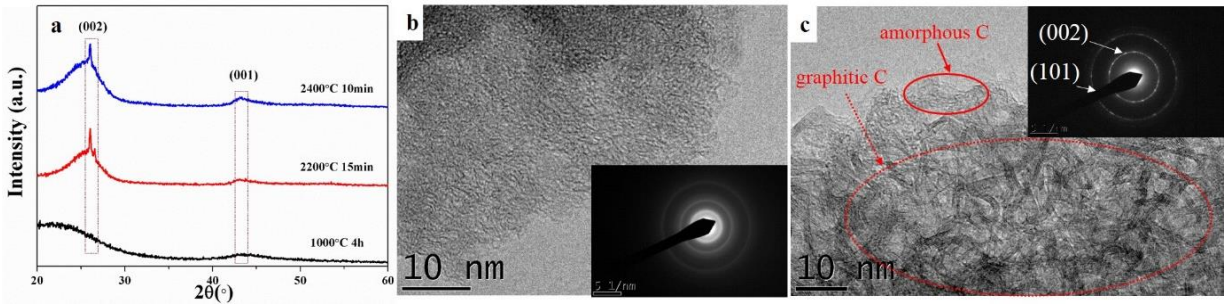

Fig.3. (a) XRD patterns of biocarbon structures obtained using different temperatures and dwell times. (b) and (c) are high resolution transmission electron microscope (HRTEM) images of the biocarbon structures prepared at 1000ºC and 2400ºC, respectively. The insets are the corresponding selected area electron diffraction (SAED) patterns.

X-ray photoelectron spectroscopy (XPS) was used to identify the chemical states of the carbon, as shown in Supplementary Fig.S1. The XPS survey spectra shown in Fig.S1a indicates the presence of C and O in both the biocarbon-1000 ºC and biocarbon-2400ºC. The biocarbon-2400ºC exhibited a smaller atomic percentage of O (3.6At%) than the biocarbon-1000 ºC (9.7At%). In the high-resolution C 1s spectra (Fig.S1 b and c), the higher dominant peak at 285.6 eV indicates a higher volume of C=C/C-C in the biocarbon-2400 ºC. Both biocarbon-

1000 ºC and biocarbon-2400ºC exhibited the peaks of C-O and C=O, which are further confirmed in the high resolution O 1s spectra (Supplementary Fig.S2).

Table 1 shows the weight loss, density, specific surface area, electrical conductivity, thermal conductivity, crystallinity ratio and compressive strength of the biocarbons. The biocarbon-1000 ºC exhibited a bulk density of 0.51g/cm^3 and a solid density of 1.85g/cm^3. The bulk density of the graphitized biocarbons-2200-2400ºC exhibited a slight decrease (from 0.51 to 0.48 g/cm^3), owing to a further weight loss of ~10wt%, probably caused by a mild oxidation of the carbon in the SPS chamber during the high temperature graphitization process. However, the solid density of the graphitized biocarbons-2200 and -2400ºC moderately increased to ~2.02g/cm^3, owing to the disappearance of nanopores and rearrangement of carbon during the graphitization process at high temperatures (2200-2400ºC). The specific surface area and specific pore volume of graphitized biocarbon-2400°C compared to the biocarbon-1000ºC decreased from 356 to 144 m^2/g and from 0.267 to 0.232 cm^3/g, respectively, owing to the disappearance of micropores (<50nm) shown in Fig.1e. Compared to biocarbon-1000ºC (~2.8 S/cm), the electrical conductivity of the graphitized biocarbons increased by ten fold (~29 S/cm). This increase was produced by the formation of the graphitic carbon, which is confirmed by the increase of the calculated crystallinity ratio of the graphitized samples given in Table 1. In addition, the compressive strength (36MPa) of the graphitized samples increased by ~38% compared to biocarbon-1000°C, again probably resulting from the graphitic carbon formed at 2200-2400ºC. However, the increased duration time from 2 to 15min and higher temperature from 2200 to 2400 ºC, did not significantly increase their compressive strength.

Table 1 The weight loss, bulk density, specific surface area, electrical conductivity, thermal conductivity and compressive strength of wood-derived biocarbon prepared at different conditions.

Heat treatment condition	Weight loss (wt%)	Bulk density (g/cm^3)	Solid density (g/cm^3)	Specific surface area (m^2/g)	Specific pore volume (cm^3/g)	RT electrical conductivity (S/cm)	RT thermal conductivity (W/(m·K))	Crystallinity ratio β	Compressive strength (MPa)
1000°C, 4h, Ar	76.6±0.1	0.51±0.02	1.85±0.03	356	0.267	2.8±0.8	1.3	0.25	26±1
2200°C, 2min, Ar	86.7±0.1	0.49±0.03	2.03±0.05	--	--	24±0.7	5.2	0.48	35±1
2200°C, 10min, Ar	87.5±0.2	0.47±0.02	2.04±0.03	--	--	25±1	6.0	0.48	34±2
2200°C, 15min, Ar	85.1±0.1	0.47±0.02	2.03±0.02	--	--	29±0.8	6.1	0.52	36±2
2400°C, 10min, Ar	85.2±0.1	0.48±0.04	2.02±0.04	144	0.232	24±0.5	6.2	0.49	36±2

Note: Heat treatment conditions refer to the highest temperature and its corresponding duration time, and heating atmosphere. The weight loss is relative to the starting wood.

Fig.4 shows the thermal transport properties versus temperatures (25-800°C) for the wood-derived biocarbon structures prepared at different temperatures (1000-2400°C) and duration times (2-15min). As shown in Fig.4a, the measured thermal diffusivity of biocarbon-1000ºC slightly increased with the measuring temperature increasing from 25 to 800ºC. On the contrary, the graphitized biocarbons exhibited decreasing thermal diffusivity with increasing

temperature. These thermal diffusivity trends versus measuring temperature are consistent with the reported data for Fe-graphitized biocarbons in the literature [8]. Compared to amorphous biocarbon-1000ºC, the graphitized biocarbons-2200ºC and -2400ºC exhibited much higher thermal diffusivity (up to ~6mm^2/s). As shown in Fig.4b, the graphitized biocarbon-2400ºC exhibited similar thermal diffusivity during the heating and cooling process, indicating the stability of the samples during the high-temperature measurements (below 800ºC).

Fig.4c shows the corresponding thermal conductivity calculated based on the measured diffusivity (Fig.4a) and using values for the heat capacity reported in the literature [15]. All of the samples exhibited increasing thermal conductivity with increasing measuring temperature from 25 to 800°C. This phenomenon is consistent with the reported results for Fe-graphitized biocarbon structures [8]. The total thermal transfer of the porous biocarbon was mainly through the pores by radiation and struts (pore walls) by electrons and phonons. The contribution of large pores (~1-500μm) to heat loss by radiation plays a significant role in the thermal transport of porous ceramic foams [22], resulting in the increase of thermal conductivity of biocarbon with increasing measuring temperature. The thermal conductivity of biocarbon-2400ºC is up to 5 times higher than the biocarbon-1000ºC at the same measurement temperature. As polycrystalline graphite has more than two orders higher thermal conductivity than amorphous carbon [23], this higher thermal conductivity of graphitized biocarbon mainly resulted from the formation of graphitic carbon. With the increase of duration time from 2 to 15min at 2200ºC, the thermal conductivity of samples increased moderately by ~12%. This mainly resulted from the increased degree of crystallinity of the biocarbon. The electronic contribution of the thermal conductivity (estimated using Wiedemann-Franz law) in the biocarbon-2400°C was estimated to be only < ~0.004 W/m/K [8] , which is far smaller than the total thermal conductivity (≥ ~2 W/m/K).

Fig.4d shows the comparison of our results with the reported thermal conductivity data for graphitized biocarbon structures derived from beech wood from the literature [8, 17]. Our samples exhibited ~72% higher thermal conductivity than the highest result reported in the literature [8, 9]. Since the crystallinity ratio of graphitized biocarbon in our work is similar to the reported one for Fe-graphitized biocarbon [8], the high thermal conductivity of our graphitized biocarbon might result from the increased phonon contributions produced by the massively reduced micropore and nanopore volumes (as shown in the BET data in Fig. 1).

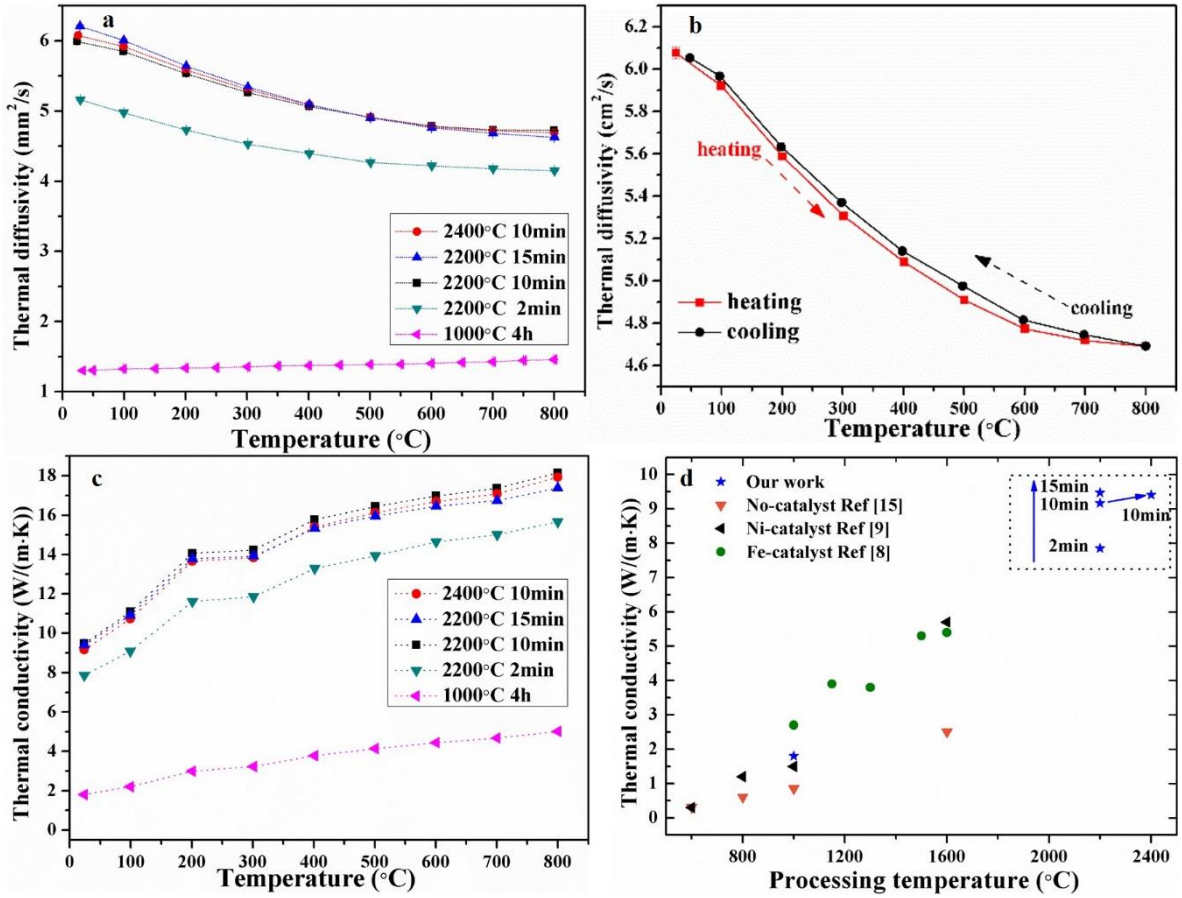

Fig.4. (a) Thermal diffusivity as a function of measuring temperatures for biocarbons obtained using different processing temperatures and dwell time. (b) The thermal diffusivity versus measuring temperatures during the heating and cooling process of the biocarbon prepared at 2400°C for 10min. (c) Thermal conductivity as a function of measuring temperatures for biocarbons. (d) Comparison of thermal conductivity (at 100ºC) of beech-derived biocarbons prepared using different techniques.

4. Conclusions

The wood-derived porous monolithic biocarbon structures was graphitized without the use of a catalyst at 2200-2400°C with high heating and cooling rates (up to 200°C/min) in a Spark Plasma Sintering (SPS) furnace. The effects of temperatures and duration time on the microstructures of the biocarbons were investigated in detail. Furthermore, the properties of the graphitized biocarbons were also investigated including their mechanical, electrical, and thermal properties. Compared to the un-graphitized biocarbon, the graphitized biocarbons at 2200ºC and 2400ºC exhibited an increased compressive strength of ~38%, and increased room-temperature electrical conductivity of ~8 fold. In addition, the graphitized biocarbons exhibited up to 5 times higher thermal conductivity than the ungraphitized biocarbon. With the increase of duration time from 2 to 15min at 2200°C, the graphitized biocarbon exhibited increased thermal conductivity by ~12%, while for the increase of temperature from 2200 to 2400°C for 10min, the graphitized biocarbon exhibited similar thermal conductivity. This indicates that 2200°C might be the optimum temperature for non-catalytic graphitization of wood-derived biocarbon.

Acknowledgement
M.Y. gratefully acknowledge the support of the European Union's Horizon 2020 Programme through a Marie Skłodowska-Curie Innovative Training Network ('CoACH-ETN", http://www.coach-etn.eu/, g.a. no. 642557). M.J.R. would like to acknowledge the support of Sunchon National University, South Korea, through the BK21+ programme and EPSRC (EP/K008749/1, XMat). T.S. was supported by EC FP7 2007-2013 (ADMACOM).

Reference

[1] E. Vogli, H. Sieber, P. Greil, Journal of the European Ceramic Society 22(14) (2002) 2663-2668.
[2] T. Wilkes, M. Young, R. Sepulveda, D. Dunand, K. Faber, Scripta Materialia 55(12) (2006) 1083-1086.
[3] C. Rambo, J. Cao, O. Rusina, H. Sieber, Carbon 43(6) (2005) 1174-1183.
[4] V. Yukhymchuk, V. Kiselov, M.Y. Valakh, M. Tryus, M. Skoryk, A. Rozhin, S. Kulinich, A. Belyaev, Journal of Physics and Chemistry of Solids 91 (2016) 145-151.
[5] H.-M. Cheng, H. Endo, T. Okabe, K. Saito, G.-B. Zheng, Journal of Porous Materials 6(3) (1999) 233-237.
[6] S.A. Steiner III, T.F. Baumann, B.C. Bayer, R. Blume, M.A. Worsley, W.J. MoberlyChan, E.L. Shaw, R. Schlögl, A.J. Hart, S. Hofmann, Journal of the American Chemical Society 131(34) (2009) 12144-12154.
[7] F. Maldonado-Hódar, C. Moreno-Castilla, J. Rivera-Utrilla, Y. Hanzawa, Y. Yamada, Langmuir 16(9) (2000) 4367-4373.
[8] J. Ramirez-Rico, A. Gutierrez-Pardo, J. Martinez-Fernandez, V.V. Popov, T.S. Orlova, Materials & Design 99(Supplement C) (2016) 528-534.
[9] M. Johnson, K. Faber, Journal of Materials Research 26(1) (2011) 18-25.
[10] M. Sevilla, A.B. Fuertes, Carbon 44(3) (2006) 468-474.
[11] D.V. Dudina, A.V. Ukhina, B.B. Bokhonov, M.A. Korchagin, N.V. Bulina, H. Kato, Ceramics International 43(15) (2017) 11902-11906.
[12] H. Guo, Y. Song, P. Chen, H. Lou, Catalysis Science & Technology (2018).
[13] C.J. Thambiliyagodage, S. Ulrich, P.T. Araujo, M.G. Bakker, Carbon 134 (2018) 452-463.
[14] C.E. Byrne, D.C. Nagle, Carbon 35(2) (1997) 267-273.
[15] A.A. Balandin, Nature materials 10(8) (2011) 569-581.
[16] M. Inagaki, J. Qiu, Q. Guo, Carbon 87 (2015) 128-152.
[17] M. Johnson, A. Childers, J. Ramirez-Rico, H. Wang, K. Faber, Composites Part A: Applied Science and Manufacturing 53 (2013) 182-189.
[18] M. Yu, E. Bernardo, P. Colombo, A.R. Romero, P. Tatarko, V.K. Kannuchamy, M.-M. Titirici, E.G. Castle, O.T. Picot, M.J. Reece, Ceramics International 44(11) (2018) 12957-12964.
[19] M. Wiener, G. Reichenauer, F. Hemberger, H.-P. Ebert, International Journal of Thermophysics 27(6) (2006) 1826-1843.
[20] H. Shang, Y. Lu, F. Zhao, C. Chao, B. Zhang, H. Zhang, RSC Advances 5(92) (2015) 75728-75734.
[21] C.H. Chia, S.D. Joseph, A. Rawal, R. Linser, J.M. Hook, P. Munroe, Journal of Analytical and Applied Pyrolysis 109 (2014) 215-221.
[22] T. Shimizu, K. Matsuura, H. Furue, K. Matsuzak, Journal of the European Ceramic Society 33(15) (2013) 3429-3435.
[23] A.A. Balandin, Nature materials 10(8) (2011) 569.